Semigeostrophic Disturbances in a Stratified Shear Flow over a Finite-Amplitude Ridge

WILLIAM BLUMEN AND BRIAN D. GROSS

Department of Astrophysical, Planetary and Atmospheric Sciences, University of Colorado, Boulder, CO 80309

(Manuscript received 17 February 1986, in final form 30 June 1986)

ABSTRACT

Steady-state, two-dimensional disturbances forced by flow over a finite-amplitude ridge are considered. The model represents an extension of the one presented by Robinson (1960). This study is based on the semigeostrophic system of equations for uniform potential vorticity flow. The model equations satisfy the Cauchy–Riemann conditions, and solutions for uniform flow over various shaped ridges may be obtained in terms of a complex potential. The novel result is the determination of solutions for disturbances in a zonal current with linear shear. The boundaries are tilted in the cross-stream direction to coincide with basic state potential temperature surfaces. This simplification, which provides isentropic boundaries, permits the solutions for disturbances in a shear flow to be obtained directly from solutions forced by uniform flow over the same ridge.

Physical properties of the solutions are presented in terms of three parameters: ϵ/D, r and δ. The amplitude of the ridge is ϵ and D is the deformation depth, based on the characteristic width of the ridge L; r represents the ratio of ϵ to the channel depth and δ is the constant shear of the basic current. Solutions corresponding to uniform flow, $\delta = 0$, in an unbounded fluid, $r = 0$, represent a limit that is compared with a previous study (Pierrehumbert, 1985). The present results confirm Pierrehumbert's conclusion that upstream deceleration is not significant, and that the characteristic vertical depth, over which the disturbances decay, is D. Confinement of the flow by a rigid lid ($r \neq 0$) and consideration of a shear ($\delta \neq 0$) do not affect that flow deceleration, nor do these features affect the characteristic decay of the ageostrophic velocity components. However, the presence of a lid causes the geostrophic velocity component to become relatively independent of depth. It is also shown that an increase in the static stability (ϵ/D increasing) enhances the ageostrophic circulation in a manner that is similar to the effect of increasing the shear δ from negative to positive values. Moreover, a linearized lower boundary condition may be used in some circumstances because the velocity components on the ridge are relatively insensitive to changes in r when $0 < r \leqslant 0.3$ and $\delta = 0$. However, linearization of the boundary condition cannot be supported when the basic flow changes with height, $\delta \neq 0$. The geostrophic momentum approximation is shown to be valid over most of the domain, but may be violated along the windward slope unless $\epsilon/D < 0.6$, with $\delta < 0.5$. Other considerations that need to be addressed to apply semigeostrophic theory to mountain flows include a stability analysis of the present solutions and the use of nonisentropic boundary surfaces.

1. Introduction

Flow over orography in rotating stratified fluid represents a problem that exhibits intrinsic mathematical and physical appeal, and not surprisingly has attracted considerable attention in atmospheric and oceanic sciences. Illuminating reviews of the subject have been presented by Smith (1979) and by various contributors to the Global Atmospheric Research Program (1980) monograph on orographic flows. The present study will focus on a particular problem that was first formulated by Robinson (1960). He considered the two-dimensional steady-state response to a uniform upstream flow forced over a finite-amplitude ridge. Only the advection of geostrophic momentum was considered by Robinson for the range of parameter values under consideration. He had, in effect, introduced the geostrophic momentum approximation for steady flows, which was later developed in greater detail for time-dependent flows by Hoskins and Bretherton (1972) and Hoskins (1975). His model was constrained to uniform potential vorticity flow and, remarkably, he showed that transformation to a streamline coordinate system provided a linear boundary value problem for finite-amplitude flow. Various extensions of Robinson's study have been presented by Jacobs (1964), Merkine (1975) and Pierrehumbert (1985), while Pierrehumbert and Wyman (1985) have recently included time-dependency and considered a parameter range for which the geostrophic momentum approximation is inapplicable.

Although the model introduced by Robinson is highly idealized, the major accomplishment is the presentation of solutions that satisfy a finite-amplitude boundary condition. The present extension of Robinson's model is the introduction of a basic upstream linear shear flow. Merkine has developed some general properties of orographic disturbances in a linear shear flow, but solutions were only presented for uniform upstream flows. The reason is that the mathematical problem is relatively difficult to solve, at least analytically, when a shear flow is present: disturbances in a uniform upstream flow satisfy isentropic boundary

conditions, a feature which may be exploited to determine solutions in a relatively straightforward manner. In the present study the boundaries are tilted in the cross-stream direction to coincide with the basic state isentropic surfaces. This simplification provides isentropic boundary conditions, yet the basic shear flow is retained.

It is clear that the model is limited by both simplifying assumptions and by the absence, for example, of a planetary boundary layer and flow around the obstacle. However, the present model solutions can be exploited to evaluate: 1) the relative importance of ageostrophic motions promoted by the presence of orography, and the characteristic spatial decay of both geostrophic and ageostrophic disturbance fields; 2) the conditions under which linearization of the lower boundary condition is appropriate; and 3) the conditions under which the geostrophic momentum approximation remains valid. These features are evaluated in terms of three physical parameters that provide measures of the ridge height relative to the channel depth, and the static stability and vertical shear of the upstream flow. Particular emphasis is placed on the role of the basic shear, which may be either positive or negative.

The present approach makes use of geostrophic coordinates (Hoskins, 1975) rather than the streamline coordinates used by the above authors. The mathematical description of the dynamics in the interior reduces to a linear problem, but the lower boundary condition remains nonlinear. There is, however, a tradeoff. It is possible to make use of the Cauchy–Riemann equations to present solutions for uniform flow over different obstacles and, most importantly, disturbances in a shear flow may be determined from the uniform flow solutions. The basic model and constraints on these solutions appear in sections 2 and 3. Solutions are presented in section 4 and various properties of the solutions appear in sections 4 and 5. Comparisons with previous studies are pointed out, as appropriate, and the present contributions are summarized in sections 5 and 6.

2. Model

A semigeostrophic, steady-state, uniform potential vorticity model is adopted. The disturbance quantities are represented as in Hoskins and Draghici (1977). The motion is two-dimensional and only depends on the geostrophic coordinates (X', Z'), defined as

$$X' = x' + v'_g/f, \quad Z' = z \tag{1}$$

where (x', z') are physical coordinates in the horizontal and vertical directions, v'_g is the cross-stream (normal to x') geostrophic velocity component, and f is the constant Coriolis parameter.

A basic geostrophic current, of characteristic amplitude U, is directed along the X' axis and contained between the ground and a rigid lid at $Z' = H$. The basic current is characterized by a constant shear $\delta' U/H$, where δ' is O(1). Thermal wind balance is maintained by a cross-stream linear variation of the basic potential temperature field. Further, the basic static stability is represented by a constant value of N, the Brunt–Väisälä frequency. Steady state finite-amplitude disturbances that can be maintained in a constant shear flow over a ridge are examined.

Pierrehumbert (1985) has shown that only one nondimensional parameter characterizes steady disturbances forced by a *uniform* flow of an unbounded atmosphere over orography.[1] This parameter is the nondimensional mountain height[2] ϵ/D, where ϵ is the characteristic amplitude of the orography and $D = fL/N$ is the so-called "deformation depth," based on the characteristic horizontal scale L of the orography. These scales will be adopted, since the uniform flow of an unbounded atmosphere represents a limit in the present development. Further, these scales apply to the geostrophic coordinates, since the deviation from physical space quantities is $O(\mathrm{Ro}) \leq 0.3$ where $\mathrm{Ro} = U/fL$ denotes the Rossby number.

The horizontal and vertical scales are $X' \sim L$ and $Z' \sim D$. All horizontal velocities are scaled by U, and the continuity equation determines the scale for the vertical velocity $w' \sim UD/L \sim 10^{-2}U$. Geostrophic balance determines the scale for the semigeostrophic potential function, $\Phi' \sim fUL$. The disturbance potential temperature θ' always appears in combination with the acceleration of gravity g and a constant reference potential temperature θ'_0; the scale, determined from the thermodynamic equation, is $g\theta'/\theta'_0 \sim fLN$.

The nondimensional basic flow is

$$u_g = 1 + \delta Z, \tag{2}$$

where $\delta = \delta' D/H \leq 1$. The nondimensional Hoskins and Draghici equations are

$$v_a^* = 0, \tag{3}$$

$$\mathrm{Ro}\, u_g \partial v_g/\partial X + u_a^* = 0, \tag{4}$$

$$\mathrm{Ro}\, v_g - \partial\, \mathrm{Ro}\Phi/\partial X = 0, \tag{5}$$

$$\theta - \partial\, \mathrm{Ro}\Phi/\partial Z = 0, \tag{6}$$

$$u_g \partial\theta/\partial X - \delta\, \mathrm{Ro}\, v_g + w^* = 0, \tag{7}$$

$$\partial u_a^*/\partial X + \partial w^*/\partial Z = 0, \tag{8}$$

$$v_a^* = v_a - \delta\, \mathrm{Ro}\, w, \quad u_a^* = u_a + \mathrm{Ro}\, w \partial v_g/\partial Z, \tag{9}$$

$$w^* = wJ^{-1}, \tag{10}$$

[1] Pierrehumbert assumes geostrophy in one direction, with the primitive equation used in the other direction. The difference with the semigeostrophic formulation is slight in the parameter range used in this study.

[2] Pierrehumbert uses the notation $\mathrm{RoFr} = (U/fL)(N\epsilon/U)$ to denote ϵ/D. His notation will not be adopted here.

where the Jacobian of the transformation to geostrophic coordinates J is defined by

$$J^{-1} = 1 - \mathrm{Ro}\partial v_g/\partial X$$
$$= (1 + \mathrm{Ro}\partial v_g/\partial x)^{-1} \quad (11)$$

and (1) becomes

$$X = x + \mathrm{Ro}v_g, \quad Z = z. \quad (12)$$

Basic-state thermal wind balance has been introduced into (7), and θ is the nondimensional representation of $g\theta'/\theta_0'$. The unique feature of this system of equations is the use of starred variables (u_a^*, v_a^*, w^*) to represent the ageostrophic velocity components (u_a, v_a) and the vertical velocity w. These definitions provide a relatively simple form for the continuity equation (8), which simplifies the present analysis. The ageostrophic component v_a may be determined from (3) and (9) but its magnitude is relatively small, $v_a \sim 10^{-1}w$, and it will not be considered.

The lower and upper boundary conditions, which have been developed in Appendix A, are

$$w^* = \frac{\epsilon}{D}(u_g + u_a^*)\frac{\partial h}{\partial X} + \mathrm{Ro}\delta^* v_g\left(1 + \frac{u_a^*}{u_g}\right), Z = \frac{\epsilon}{D}h(X) \quad (13)$$

$$w^* = \mathrm{Ro}\delta^* v_g\left(1 + \frac{u_a^*}{u_g}\right), \quad Z = \frac{H}{D}, \quad (14)$$

where $h(X)$ represents the shape of the ridge, and a constant cross-stream slope of both boundaries $\mathrm{Ro}\delta^*$ ($\delta^* < 1$) has been introduced for mathematical convenience. Solutions have only been obtained for the case when both boundaries are isentropic surfaces; this is equivalent to $\delta^* = \delta$. However, $\delta^* \neq \delta$ will be retained for the present to show how this simplification is introduced.

All disturbances are required to vanish when the upper lid is removed, $Z = H/D \to \infty$. Disturbances also vanish upstream. In particular v_g satisfies

$$v_g \to 0, \quad X \to -\infty. \quad (15)$$

The downstream condition will be examined in conjunction with the solution.

The Ro only appears in combination with Φ, and may be absorbed into the definition of Φ as noted by Pierrehumbert. The nondimensional parameters that have been introduced are the ridge height, ϵ/D, the basic velocity shear, δ, the channel depth, H/D, and δ^*, which is proportional to the cross-stream slope of the boundary surfaces. Some other parameters will arise in the lower boundary representation, so that the range of these parameter values will not be considered here.

3. Formulation of the boundary-value problem

The interior uniform potential vorticity flow satisfies

$$\partial^2\Phi/\partial X^2 + \partial^2\Phi/\partial Z^2 = 0, \quad (16)$$

as shown by Hoskins (1975).

Substitution of (5) and (6) and, respectively, (13) and (14) into the thermodynamic equation (7) yields

$$u_g\frac{\partial^2 \mathrm{Ro}\Phi}{\partial X\partial Z} - (\delta - \delta^*)\frac{\partial \mathrm{Ro}\Phi}{\partial X} + \frac{\epsilon}{D}(u_g + u_a^*)\frac{dh}{dX} + \left(\delta^*\frac{u_a^*}{u_g}\right)\frac{\partial \mathrm{Ro}\Phi}{\partial X} = 0, \quad Z = \frac{\epsilon}{D}h(X) \quad (17)$$

$$u_g\frac{\partial^2 \mathrm{Ro}\Phi}{\partial X\partial Z} - (\delta - \delta^*)\frac{\partial \mathrm{Ro}\Phi}{\partial X} + (\delta^* u_a^*/u_g)\frac{\partial \mathrm{Ro}\Phi}{\partial X} = 0, \quad Z = H/D. \quad (18)$$

The difference between the slope of the basic state isentropic surfaces and the sloping boundaries is measured by $\delta - \delta^*$. Analytic solutions could not be obtained when these sloping boundaries intersect, so that basic state isentropic boundaries, $\delta = \delta^*$, are considered. Further simplification is introduced by noting that the last term in (17) may be neglected if $\delta\ \mathrm{Ro}/(\epsilon/D) \ll 1$. This latter ratio may be expressed as

$$\delta'\frac{\epsilon}{H}(fUL/N^2\epsilon^2) \ll 1,$$

with $\delta' \leqslant 1$ and $\epsilon/H \leqslant 0.3$. This inequality requires that the characteristic geostrophically balanced pressure difference not exceed the characteristic hydrostatic pressure difference over the vertical extent of the ridge.

It is convenient to introduce an ageostrophic disturbance streamfunction ψ, such that

$$u_a^* = -\frac{\partial\psi}{\partial Z}, \quad w^* = \frac{\partial\psi}{\partial X} \quad (19)$$

satisfy (8). The case $\delta = 0$ is considered first. Introduction of $w^* = \partial\psi/\partial x$ into (7), followed by integration of the expression, provides

$$\psi = -\theta = -\frac{\partial \mathrm{Ro}\Phi}{\partial Z}. \quad (20)$$

The lower boundary condition (13) may now be expressed as

$$d(Z - \psi) = 0, \quad Z = \frac{\epsilon}{D}h(X) \quad (21)$$

with the aid of (19). Comparison of (20) and (21), confirms that the lower boundary is an isentrope, $Z + \theta$ = constant.

Now consider $\delta \neq 0$. Introduction of (5) and $w^* = \partial\psi/\partial X$ into (7) leads to the expression

$$\psi = \delta\,\mathrm{Ro}\Phi - (1 + \delta Z)\frac{\partial \mathrm{Ro}\Phi}{\partial Z}. \quad (22)$$

Introduction of (22) into (17) yields

$$-\frac{\partial^2 \mathrm{Ro}\Phi}{\partial X \partial Z}=\left(1+\frac{\partial^2 \mathrm{Ro}\Phi}{\partial Z^2}\right)\frac{\partial h}{\partial X},$$

which is equivalent to

$$d\left(Z+\frac{\partial \mathrm{Ro}\Phi}{\partial Z}\right)=0, \quad Z=\frac{\epsilon}{D}h(X). \tag{23}$$

The lower boundary in this case ($\delta = \delta^*$) is also an isentrope, but the disturbance streamfunction ψ is determined by (22).

Now, if (4) and (5) are introduced into (18), integration shows that the upper boundary may be represented as

$$u_g\frac{\partial \mathrm{Ro}\Phi}{\partial Z}-\delta(\mathrm{Ro}v_g)^2/2=\text{constant}, \quad Z=H/D. \tag{24}$$

The second term may be neglected if $\delta\ \mathrm{Ro} \ll 1$, with $u_g \sim 1$. Consequently, the upper boundary condition reduces to

$$\theta=\partial \mathrm{Ro}\Phi/\partial Z=\text{constant}, \quad Z=H/D. \tag{25}$$

It follows that, when the boundaries can be represented as isentropic surfaces, *any solution Φ found for uniform flow over a ridge is also the solution in a shear flow over the same ridge, but the ageostrophic solution ψ is determined by* (22) *with* $\delta \neq 0$.

4. Solutions

Solutions corresponding to *uniform* flow between isentropic boundary surfaces will be considered first, since these solutions are required to determine the ageostrophic response to a vertical shear flow. When $u_g = 1$, (4) and (7) reduce to

$$u_a^*=-\frac{\partial \mathrm{Ro}v_g}{\partial X}, \tag{26a}$$

$$w^*=-\frac{\partial \mathrm{Ro}v_g}{\partial Z}, \tag{26b}$$

where (5) and (6) have been used to introduce v_g into (26b). Introduction of (12) and (19) into (26a, b) provides the equivalent expressions

$$\partial x/\partial X=\partial \Psi/\partial Z, \tag{27a}$$

$$\partial x/\partial Z=-\partial \Psi/\partial X, \tag{27b}$$

where $\Psi = Z - \psi$. Since the present system of equations satisfy the Cauchy–Riemann conditions (27a, b), the solution may be expressed in terms of a complex potential F, defined as

$$F=x(\zeta)+i\Psi(\zeta), \tag{28}$$

where F is an analytic function of the complex variable

$$\zeta=X+iZ. \tag{29}$$

The boundary conditions (21) and (25) reduce to

$$\Psi=\Psi_0, \quad Z=\Psi_0+\frac{\epsilon}{D}h(X) \tag{30a}$$

$$\Psi=\Psi_1, \quad Z=\Psi_0+H/D \tag{30b}$$

where (Ψ_0, Ψ_1) are constants, and the reference level $Z = \Psi_0$ has been included in (30a, b) for convenience.

A ridge will be *constructed* by introduction of a source at $\zeta = -a$ and a sink at $\zeta = a$, which are placed at the bottom of a channel capped by a rigid lid at $Z = \Psi_0 + H/D$. A uniform current ($\delta = 0$) directed along the X-axis may be added to the flow field and the total complex potential represented as (Milne–Thomson, 1950; §10.4)

$$F(\zeta)=\zeta+m\ln\{\sinh[\pi D(\zeta+a)/2H]\}-m\ln\{\sinh[\pi D(\zeta-a)/2H]\}, \tag{31}$$

where m represents the source and the sink strength. Here, F and m are nondimensional variables, and both are scaled by UD. In this representation (31) the ratio m/a plays the role of an aspect ratio for the ridge. Numerical evaluation of the real and imaginary parts of $F(\zeta)$ is required to obtain the flow field. However, an analytical result may be obtained for a limiting case, and this solution provides a physical background that aids in the interpretation of the solution provided by (31). The reader may, however, bypass the remainder of this section and pick up the development in section 5, where the numerical results are presented.

A limiting value of F may be obtained by considering a doublet at the origin ($\zeta = 0$): $\mu^2 = 2ma$ remains finite as $a \to 0$. Then (31) reduces to

$$F=\zeta+\mu^2(\pi D/2H)\coth(\pi D\zeta/2H). \tag{32}$$

Separation of the real and imaginary parts of (32), according to (28) and (29), yields

$$x=X+\mu^2\frac{\pi D}{2H}\frac{\sinh(\pi DX/2H)\cosh(\pi DX/2H)}{\sin^2(\pi DZ/2H)+\sinh^2(\pi DX/2H)}, \tag{33a}$$

$$\Psi=Z-\mu^2\frac{\pi D}{2H}\frac{\sin(\pi DZ/2H)\cos(\pi DZ/2H)}{\sin^2(\pi DZ/2H)+\sinh^2(\pi DX/2H)}. \tag{33b}$$

The lower boundary is provided by (33b) with $\Psi = \Psi_0$. The physical space representation reduces to an elliptic cylinder when $H \to \infty$ and $\Psi_0 = 0$, as shown in Appendix B.

The cross-stream geostrophic velocity, $\mathrm{Ro}v_g = X - x$, is given by

$$\mathrm{Ro}v_g=-\mu^2\frac{\pi D}{2H}\frac{\sinh(\pi DX/2H)\cosh(\pi DX/2H)}{\sin^2(\pi DZ/2H)+\sinh^2(\pi D/2H)}+\text{constant}. \tag{34}$$

The addition of an arbitrary constant into (34) does

not restrict the solution in any way, but its presence is required in order to satisfy the upstream condition $v_g \to 0$ as $X \to -\infty$. The solution for v_g is

$$\mathrm{Ro} v_g = -\mu^2 \frac{\pi D}{2H}\left[1 + \frac{\sinh(\pi DX/2H)\cosh(\pi DX/2H)}{\sin^2(\pi DZ/2H) + \sinh^2(\pi DX/2H)}\right] \tag{35}$$

and, from $\Psi = Z - \psi$, the disturbance streamfunction is

$$\psi = \mu^2 \frac{\pi D}{2H} \frac{\sin(\pi DZ/2H)\cos(\pi DZ/2H)}{\sin^2(\pi DZ/2H) + \sinh^2(\pi DX/2H)}. \tag{36}$$

These solutions satisfy all the boundary conditions, (15) and (30a, b), and the presence of the upper lid imposes a permanent downstream deflection of the cross-stream velocity component. This latter feature was first pointed out by Jacobs (1964).

Results from the numerical evaluation of the solution (31), which takes account of both the source–sink strength and the separation a, will be presented in section 5.

a. Ageostrophic velocity over the ridge crest

Flow over the (physical space) semicircular ridge (B1), in Appendix B, is associated with two properties of the solution that invalidate the present model: namely, an infinite ageostrophic velocity at the ridge crest and an infinite relative vorticity (a stagnation point) at the base of the ridge. Flow over a broader ridge (B5) avoids the infinite velocity at the crest, but the stagnation point remains.

Here the rigid lid is retained, and a streamline $\Psi = \Psi_0 \neq 0$ in (33a) represents the ridge. Introduction of (35) into (4), and evaluation at the ridge crest ($X = 0$, $Z = z = \Psi_0 + \epsilon/D$) where $w = 0$, yields

$$u_a = u_g(\mu\pi D/2H)^2/\sin^2(\pi Dz/2H). \tag{37}$$

Evaluation of (33b) at the crest leads to an expression for the doublet strength μ^2 that corresponds to a specified value of the ridge amplitude,

$$(\mu\pi D/2H)^2 = \frac{\epsilon}{D}(\pi D/2H)\tan(\pi Dz/2H), \quad z = \Psi_0 + \frac{\epsilon}{D}. \tag{38}$$

Elimination of μ^2 between (37) and (38) provides the expression

$$u_a = u_g \frac{\epsilon}{D}(\pi D/H)/\sin(\pi Dz/H), \quad z = \Psi_0 + \frac{\epsilon}{D}. \tag{39}$$

This result (39) is also valid for $u_g = 1 + \delta z$, since the expression in (33b) is equivalent to the lower boundary condition (23) that applies when $\delta \neq 0$. Consequently, it is preferable to associate Ψ_0 with a constant isentropic boundary at $|x| = \infty$ rather than a streamfunction.

The limiting case, $H \to \infty$ and $\Psi_0 \to 0$, yields the maximum value of u_a in an unbounded fluid, namely $u_a = u_g$. This is also the approximate value for a small-amplitude ridge. However, when H is finite, u_a increases monotonically until the peak touches the upper lid, at which point $u_a = \infty$. The variation of the peak value of u_a is shown in Fig. 1 as a function of $r = \epsilon/H$, the ratio of the ridge amplitude to channel depth. A realistic upper limit, corresponding to $H \approx 10$ km, is $r = 0.3$. The maximum value of u_a in this case is about 16 percent higher than the value associated with a linear boundary condition. However, if u_g doubles in magnitude between the level ground and the lid, the value of u_a associated with $r = 0.3$ will be over 50 percent higher than the linear value; a decrease of u_g to zero at the lid will give approximately a 19 percent lower value at the ridge crest.

The variation of u_a above the crest ($x = 0$) may be determined from (37), since $w = 0$ at all levels for a symmetrical ridge. The doublet strength μ is determined from (38), but $\Psi_0 + \epsilon/D \leq z \leq H/D$. Profiles of $u_a(z)$ are displayed in Fig. 2 for various values of the basic shear δ and $r = 0.15$. Although the magnitude u_a is controlled by u_g, the characteristic depth scale D of u_a, discussed by Pierrehumbert (1984), is not significantly affected by the presence of $\delta \neq 0$ for the parameter values considered. Only values of $|\delta| \gg 1$ could affect this depth scale for u_a, but these values violate the condition $|\delta| \leq 1$ established in section 3.

Although the doublet ridge (33b) alleviates the problem of an infinite velocity at the ridge crest, more flexibility in the specification of the ground surface is desirable. This will be achieved in section 5 by choosing $\Psi_0 \neq 0$, and by varying the source strength m and the separation a in order to introduce adjustable aspect ratios (vertical to horizontal axes).

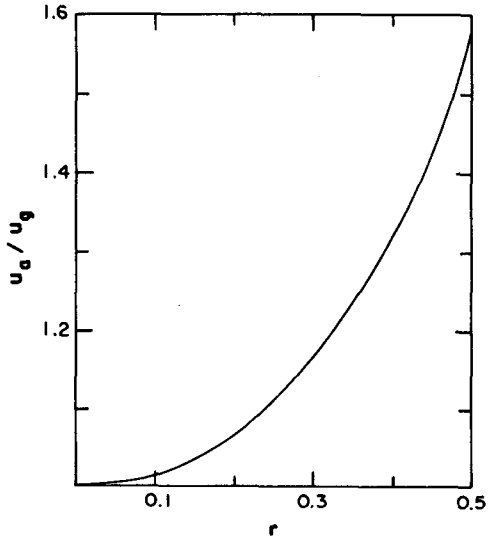

FIG. 1. Variation of the ageostrophic wind u_a, given by (39), at the crest of a ridge as a function of $r = \epsilon/H$. The ridge is represented by (33b) with $\Psi = \Psi_0 = 0$.

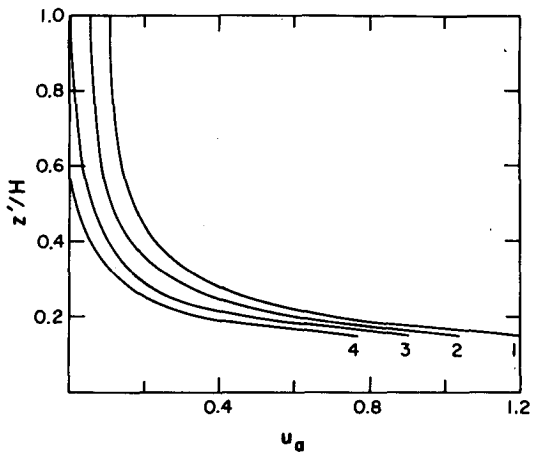

FIG. 2. Variation of the ageostrophic wind u_a above the ridge crest as a function of nondimensional height z'/H, where $z' = zD$. The ridge is represented as in Fig. 1; the crest is situated at $z'/H = r = 0.15$, and the lid is at $z'/H = 1$. The curves correspond to different values of the basic shear δ according to 1) $\delta = 0.375$, $u_g(1) = 2$; 2) $\delta = 0$, $u_g(1) = 1$; 3) $\delta = -0.375$, $u_g(1) = 0$; 4) $\delta = -0.65$, $u_g(1) = -0.73$. Curve 4 reaches a minimum value at the lid equal to $u_g(1) = -0.04$.

b. Stagnation points

The existence of stagnation points, where $u_g + u_a = 0$, at the base of the ridge are not acceptable since the relative vorticity is infinite, $\partial \, \mathrm{Ro} v_g/\partial x = \infty$. This feature is exhibited in Appendix B in association with the semicircular ridge (B1). Although the ridge given by (33b) is broader, stagnation points occur at discontinuities in the boundary slope when $\Psi_0 = 0$. However, it will be shown that this latter problem can be eliminated by requiring $\Psi_0 \neq 0$.

The infinity in the relative vorticity, associated with $u_g + u_a = 0$, may also be expressed as $\partial \, \mathrm{Ro} v_g/\partial X = 1$ from the coordinate transformation provided in (11). Evaluation by means of (35) leads to

$$[\sin^2(\pi DZ/2H) + \sinh^2(\pi DX/2H)]^2 + (\mu\pi D/2H)^2 \times \{[\cosh^2(\pi DX/2H) + \sinh^2(\pi DX/2H)] \times [\sin^2(\pi DZ/2H) + \sinh^2(\pi DX/2H)] - 2\sinh^2(\pi DX/2H)\cosh^2(\pi DX/2H)\} = 0. \quad (40)$$

Now (33b) may be expressed as

$$\sinh^2(\pi DX/2H) = (\mu^2\pi D/2H)\frac{\sin(\pi DZ/2H)\cos(\pi DZ/2H)}{Z-\Psi_0} - \sin^2(\pi DZ/2H). \quad (41)$$

Substitution of (41) into (40), and reduction by means of trigonometric identities, produces the result

$$\mu^2[\tan(\pi DZ/H) - (Z-\Psi_0)(\pi D/H)] = -2(Z-\Psi_0)^2\tan(\pi DZ/H), \quad (42)$$

where $Z - \Psi_0 \leq Z$. In the range $0 < Z \leq H/2D$, where $\tan\pi DZ/H > 0$, (42) cannot be satisfied; when $H/2D \leq Z \leq H/D$, where $\tan\pi DZ/H \leq 0$, (42) cannot be satisfied. The only values that satisfy (42) are $Z = \Psi_0 = 0$ and, according to (40), this choice is associated with $|X| = \mu$. These points are located at discontinuities of the slope of the lower boundary. The simplest demonstration of this feature is exhibited by the intersection of the elliptical ridge (B5) with $z = 0$, which occurs at $|x| = 2\epsilon/D$. In this case the streamline at $z = 0$ ($\Psi_0 = 0$) is the dividing streamline for flow around the elliptic cylinder. In general, the fact that (40) cannot be satisfied when $\Psi_0 \neq 0$ implies that the flow cannot be decelerated to zero by any value of ϵ/D. In addition, the upstream region of deceleration of u_a at low levels is the order of ϵ/D, which agrees with Pierrehumbert's (1985) estimate.

5. Numerical evaluation

The complex potential (31) for uniform flow ($\delta = 0$) may be separated into real and imaginary parts to give the expressions

$$x = X + m\ln\left\{\frac{\sinh^2[\pi D(X+a)/2H] + \sin^2(\pi DZ/2H)}{\sinh^2[\pi D(X-a)/2H] + \sin^2(\pi DZ/2H)}\right\}, \quad (43a)$$

$$\Psi = Z - \psi = Z - 2m\tan^{-1}\left\{\frac{\sinh 2(\pi Da/2H)\sin 2(\pi DZ/2H)}{\cosh 2(\pi DX/2H) - \cosh 2(\pi Da/2H)\cos 2(\pi DZ/2H)}\right\}. \quad (43b)$$

The method of solution for $\delta \neq 0$ is presented in section 3. The constant Ψ_0, in (30a), is defined as

$$\Psi_0 = qH/D = q\frac{\epsilon}{D}\Big/ r(1-q), \quad (44)$$

where

$$r(q) \equiv \epsilon/(1-q)H \quad (45)$$

and $q \ll 1$ is a constant.

Determination of the lower boundary in terms of the parameters m, a, ϵ/D and $r(q)$ is presented in Appendix C. Both ϵ/D and $r(q)$ are constrained to a range of values that depend on the separation a and the constant q. For example, this range is bounded by the two curves in Fig. 3, when $q = 0.1$. The upper curve represents zero separation (doublet), while a varies along the lower curve as pointed out in Appendix C. The source–sink strength m is then determined by known values of a, ϵ/D and $r(q)$ for the chosen value of q. The slopes of the ridges determined by this procedure are not identical for the same value of ϵ/D: the x coordinate

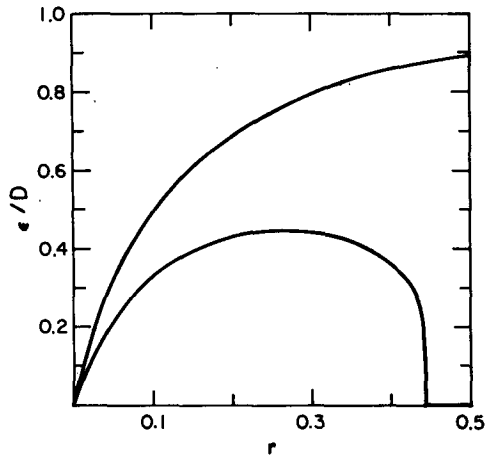

FIG. 3. Allowable parameter values of ϵ/D and $r = \epsilon/H$ fall between the solid curves, constructed for the case $q = 0.1$ in (44). This parameter range, a function of the source/sink strength m and their separation a, is determined in Appendix C.

is stretched relative to the X coordinate in the transformation to physical space, and the difference between their positions depends on $r(q)$. However, those differences are not significant when $0.1 \leqslant q \leqslant 0.2$. Hereafter $r(q) \equiv r$ will be used for simplicity. The remaining constraints on parameter values, specified previously, are

(i) $r \leqslant 0.3$,

(ii) $\epsilon/D < 1$, $(\mathrm{Ro} \leqslant 0.3)$

(iii) $\delta < 1$.

Figures 4–7, display various (x, z) cross sections that illustrate properties of the solutions in terms of these three parameters.

a. *Variation of r*

The parameter r, given by (45), measures variations in the channel depth for fixed values of ϵ, and drops out of the problem when the fluid is unbounded. The principal effect from varying r is displayed in Fig. 1. The ageostrophic velocity component u_a must increase monotonically with r to maintain a constant flux of mass over the ridge. The spatial distribution of $u_a(x, z)$ is shown in Fig. 4 for $r = 0.075$ and $r = 0.3$. These ridges are represented by streamlines above an elliptic cylinder whose major axis coincides with $z = 0$. Consequently, the lower peak values of u_a in Fig. 4, compared to those in Fig. 1 for the same value of r, are indicative of the decay of u_a with height displayed in Fig. 2. The results in Fig. 4 show that upstream and downstream deceleration, $u_a < 0$, is not significant. The explanation is associated with the specification $\Psi_0 \neq 0$, which eliminates any evidence of the stagnation point that occurs when the bottom slope is discontinuous. In fact, the relatively small deceleration for smooth boundary profiles and the stagnation point associated with a discontinuous profile, found by Pierrehumbert (1985), may be interpreted as above. His results represent flows over symmetric obstacles, as in this study, because the Cauchy–Riemann equation is satisfied by his solutions.

Another feature associated with a lid is the upwind displacement of the $v_g = 0$ contour, shown in Fig. 5. This feature arises because a constant velocity $v_g(\infty)$ must be added to the solution, when H is finite, in order to satisfy the upstream condition $v_g(-\infty) = 0$, [e.g., see (34) and (35)]. Consequently, $v_g(0, z) = v_g(\infty, z)/2 < 0$ and the zero contour is displaced upstream. A byproduct of this result is the virtual elimination of a characteristic decay of v_g with height, which is quite apparent for $r = 0.3$ in Fig. 5. The relatively large in-

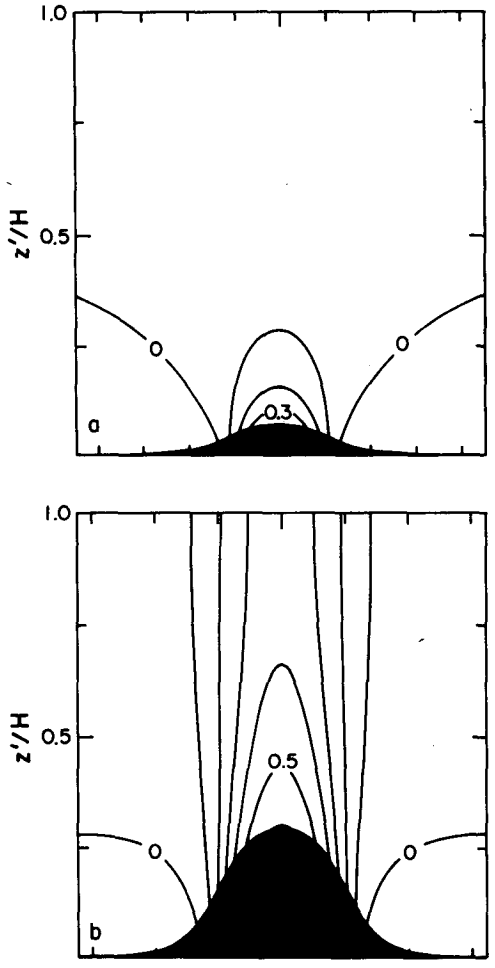

FIG. 4. Distribution of the ageostrophic wind u_a as a function of nondimensional height z'/H and horizontal distance x, expressed in nondimensional units corresponding to the half-width of the ridge shown in each panel. The relative ridge heights ϵ, expressed by $r = \epsilon/H$, are (a) $r = 0.075$ and (b) $r = 0.3$. The contour increments of u_a are 0.1 in units of the upstream geostrophic velocity u_g. The parameters are $\epsilon/D = 0.4$ and $\delta = 0$.

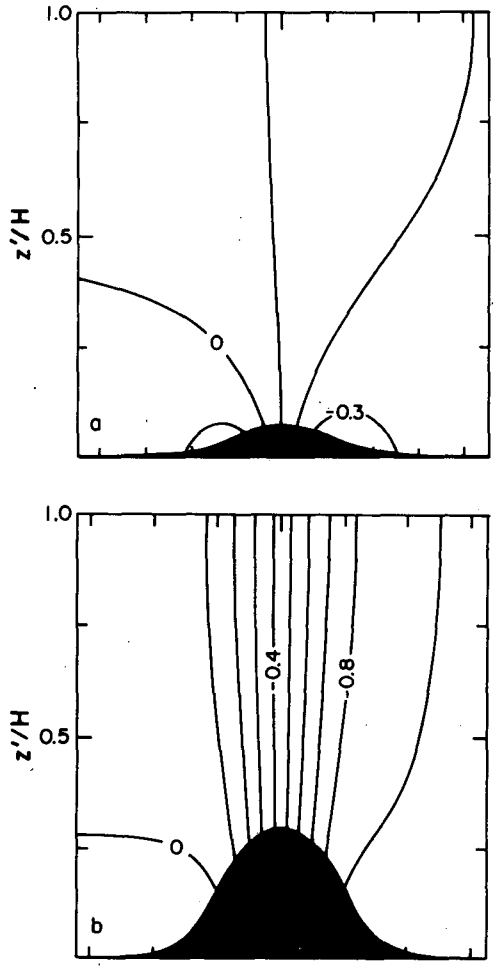

FIG. 5. As in Fig. 4, except for cross-stream geostrophic velocity $\mathrm{Ro}v_g$.

crease in $-|\partial\, \mathrm{Ro}v_g/\partial x|$, associated with an increase in r, produces the corresponding increase in u_a as required by the momentum equation (4). As r decreases, the $v_g = 0$ contour moves toward the crest and the solution approaches the one appropriate for an unbounded fluid.

A drag, exerted on the atmosphere by a ridge, was determined by Merkine [1975, Eq. (2.16)] based on the asymmetry of the cross-stream geostrophic pressure field evident in Fig. 5. Smith (1979) points out that this drag force arises from the use of an infinite ridge in an atmosphere capped by a rigid lid ($r \neq 0$). He notes that these model assumptions eliminate the "outer" decay region, far from the obstacle, that would be associated with a ridge of finite extent. This limitation of the model is responsible for the *apparent* drag that is computed in the near field region. However, the forced ageostrophic flow remains symmetric (Figs. 6 and 7) and does not contribute to the *apparent* drag, which is only associated with the geostrophic pressure field. Eliassen and Palm (1961) have examined the contribution to the drag related to the asymmetry of the ageostrophic circulation. This asymmetry is associated with wave motions that are not present in either a geostrophic or a semigeostrophic model when the Coriolis parameter is constant.

b. *Variation of* ϵ/D

The parameter ϵ/D, where $D = fL/N$, provides relative measures of the slope ϵ/L or of the static stability N for fixed f. Here the same ridge will be used, so that variations in ϵ/D imply static stability variations. Further, the present approach excludes the possibility $u_a = \infty$ when $\epsilon/D = \mathrm{O}(1)$, and the range of ϵ/D is limited as shown in Fig. 3. The range of static stability varia-

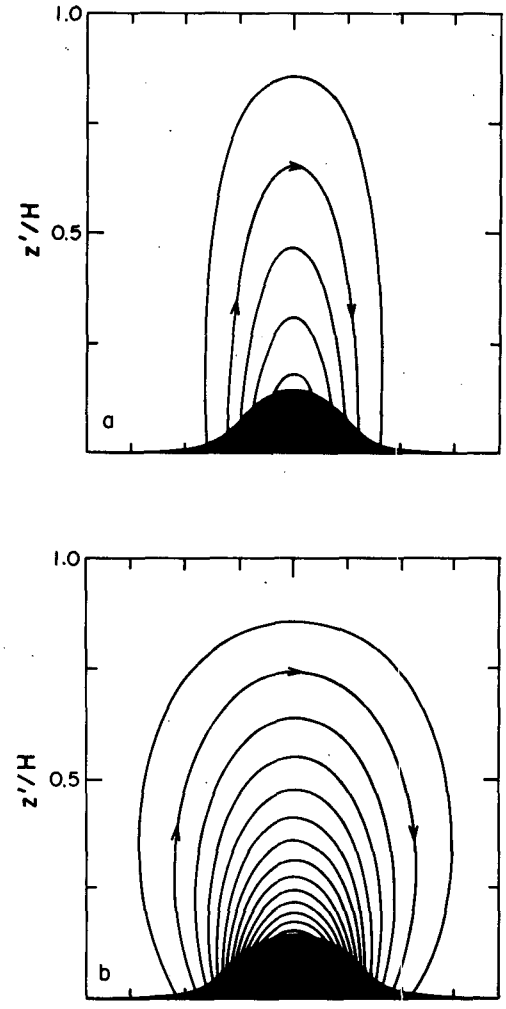

FIG. 6. Physical space streamfunction ψ, representing the ageostrophic circulation associated with (u_a, w). The parameters are $r = 0.15$ and $\delta = 0$. Relative differences in the static stability are expressed by (a) $\epsilon/D = 0.2$ and (b) $\epsilon/D = 0.6$. Corresponding temperature lapse rates appear in the text.

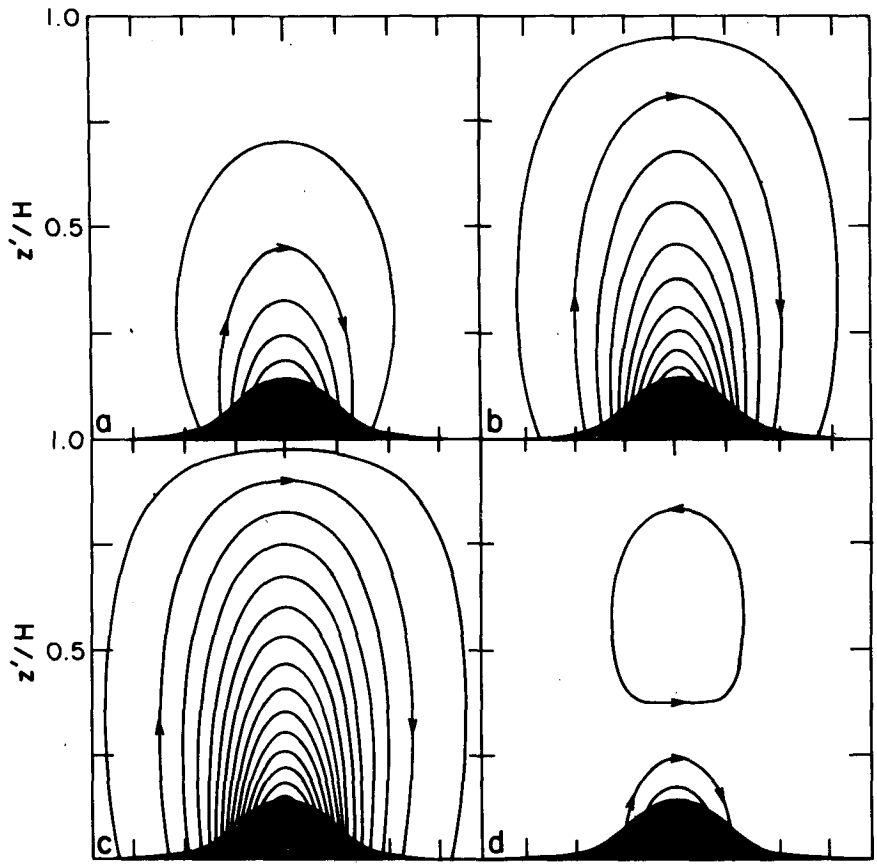

FIG. 7. Physical space streamfunction ψ representing the ageostrophic circulation. The vertical velocity associated with the cross-stream sloping boundaries has been removed. The fixed parameter values are $r = 0.15$ and $\epsilon/D = 0.4$. The panels correspond to different shears δ of the geostrophic velocity u_g according to: (a) $\delta = -0.375$, $u_g(1) = 0$; (b) $\delta = 0$, $u_g(1) = 1$; (c) $\delta = 0.375$, $u_g(1) = 2$; (d) $\delta = -0.65$, $u_g(1) = -0.73$.

tions for $0.2 \leqslant \epsilon/D \leqslant 0.6$ essentially covers typical atmospheric values. Consider

$$\frac{\epsilon}{D} = \frac{\epsilon}{H}\frac{H}{D} = r\frac{H}{D_0}\frac{N}{N_0},$$

where $D_0 = fL/N_0$. The reference value is $N_0 = 2 \times 10^{-2}\ \mathrm{s}^{-1}$, which may be associated with an isothermal atmosphere at temperature $T_0 = 250$ K. Assuming that $r = 0.15$ and $D/H = 0.2$ ($H = 10^4$ m, $L = 4 \times 10^5$ m), the lapse rates are

$$\gamma = 9.3 \times 10^{-3}\ \mathrm{K\,m^{-1}}, \quad \epsilon/D = 0.2$$

$$\gamma = 3.6 \times 10^{-3}\ \mathrm{K\,m^{-1}}, \quad \epsilon/D = 0.6.$$

The physical space streamfunctions ψ for the ageostrophic flow corresponding to these values of ϵ/D and $r = 0.15$ are shown in Fig. 6. The larger value, $\epsilon/D = 0.6$, promotes faster motion ($u_a = -\psi_z$) over the ridge since the larger stratification tends to act as a lid at lower levels: the vertical scale D varies inversely with N so, in effect, the same amount of air passes through a smaller area even though ϵ and H are same in both cases. In addition, the vertical velocity ($w = \psi_x$) must be larger on the windward and leeward slopes (and begins to rise relatively far from the crest) to satisfy continuity conditions at low levels.

c. *Variation of* δ

The presence of basic shear ($\delta \neq 0$) only affects the distributions of the ageostrophic velocities (u_a, w). This circumstance is an artifact of the boundary conditions, the requirement that the boundaries be isentropic surfaces. Vertical profiles of $u_a(z)$ for different values of δ appear in Fig. 2. The extent of the ageostrophic circulation over a ridge is exhibited in Fig. 7 for the same values of r and ϵ/D. The magnitudes of u_a associated with Fig. 7 are somewhat less than the values in Fig. 2, because $\Psi_0 \neq 0$, but the vertical variations over the crest are qualitatively similar.

Comparison between the circulations displayed in Figs. 6 and 7 reveal that there is a correspondence between relatively small ϵ/D and $\delta < 0$ and relatively large ϵ/D and $\delta > 0$. However, the reason for similarity

in these circulation differs. A relatively larger vertical motion is forced at the lower boundary when $\delta > 0$ than when $\delta < 0$, since $w \propto u_g \partial h(x)/\partial x$. However the vertical decay scale ϵ/D is essentially independent of $u_g(z)$, so that a relatively large horizontal velocity u_a must flow over the ridge crest to maintain mass continuity when $\delta > 0$, compared to the situation when $\delta < 0$. The increase in u_a is directly proportional to δ, as shown by (39) and the profiles displayed in Fig. 2. This relationship (39) between u_a and u_g also accounts for the reversal of the circulation above the level where $u_g = 0$, appearing in Fig. 7d. However, this reverse cell is weak since the ageostrophic motion is quite small at upper levels.

Interestingly, the use of a linearized lower boundary condition, $w[x, z(X)] \approx w(x, \Psi_0)$, can be justified when $\delta \approx 0$ and when $r > 0$. The reason is related to the relative constancy of v_g with height displayed, for example, in Fig. 5 for $r = 0.3$. As a consequence u_a is relatively insensitive to changes in the ridge amplitude ϵ, as is evident from (4). However, significant variability of u_a can occur when $\delta \neq 0$, as shown in Fig. 2, although the distribution of v_g is unaffected. Alternatively, v_g decays over the characteristic scale ϵ/D when $r \approx 0$, so that significant changes in the variables will occur over the vertical extent of the ridge.

6. Concluding remarks

Attention is now directed to evaluation of the geostrophic momentum approximation with the present model. Advections of ageostrophic velocity components (u_a, v_a) are neglected in (3) and (4), but those terms may be evaluated ex post facto. Consider the ratio of the dimensional terms

$$\frac{(u'_g + u'_a)\partial v'_a/\partial x'}{(u'_g + u'_a)\partial v'_g/\partial x'} \sim v'_a/v'_g.$$

Introduction of nondimensional variables and use of (3) and (9) yields

$$v'_a/v'_g \sim \mathrm{Ro}\delta \leqslant 0.1$$

for typical values of the parameters. However, this evaluation depends on the validity of geostrophic balance, expressed by (5).

The geostrophic momentum approximation is valid in the present model if (Hoskins, 1975)

$$[(u'_g + u'_a)\partial u'_a/\partial x' + w'\partial u'_a/\partial z'] \ll f v'_g.$$

The nondimensional expression is

$$\mathrm{Ro}^2[(u_g + u_a)\partial u_a/\partial x + w\partial u_a/\partial z] \ll \mathrm{Ro} v_g. \quad (46)$$

The terms appearing in (46) have been evaluated at the lower boundary for relatively extreme values of the model parameters: $\epsilon/D = 0.6$ and $\delta = 0.5$. Two different values of r, corresponding to ridge amplitudes of, say, 1.5 and 3 km in a 10-km channel, have been used in the evaluations displayed in Fig. 8. Note that there is

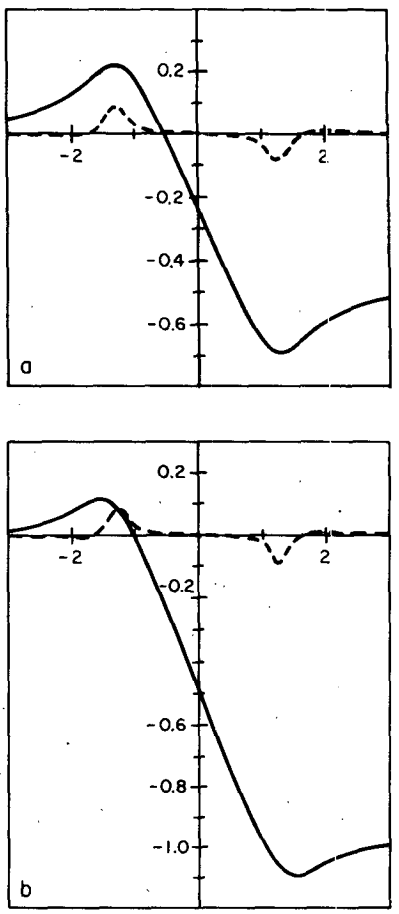

FIG. 8. Variation of the geostrophic velocity $\mathrm{Ro} v_g$ (solid) and the ageostrophic acceleration $\mathrm{Ro}^2[(u_g + u_a)\partial u_a/\partial x + w\partial u_a/\partial z]$ (dashed) along the lower boundary. The abscissa is expressed in units of the half-width of the ridges associated with $\epsilon/D = 0.6$ and the values (a) $r = 0.15$ and (b) $r = 0.30$. The basic shear is $\delta = 0.5$, corresponding to $u_g(1) = 2.33$.

a relative decrease in the magnitude of v_g on the windward slope and a relative increase on the leeward slope, associated with an increase in r. This feature is associated with the fact that the constant $v_g(\infty)$, added to the antisymmetric solution to satisfy the upstream boundary condition (15), increases with r: the downstream value of v_g increases by this added constant, and the antisymmetry in the solution is preserved by a corresponding decrease in v_g on the upstream slope.

The results in Fig. 8 show that the geostrophic momentum approximation (46) is essentially satisfied everywhere, except on the windward slope. However, in an unbounded atmosphere ($r = 0$), v_g is in phase with the ageostrophic acceleration, and the results in Fig. 8 indicate that the geostrophic momentum approximation would be satisfied for $\epsilon/D \leqslant 0.6$ in the present model. These results only represent a guide to the applicability of the geostrophic momentum approximation in orographic flows. The use of different mountain

slopes, other basic flows and the inclusion of three-dimensionality could alter the present conclusions.

The principal result obtained in the present analysis is the presentation of two-dimensional solutions for finite-amplitude disturbances in a linear shear flow over a ridge. These solutions were obtained by requiring that both the upper and lower boundaries be isentropic surfaces, which requires a cross-section tilt of these boundaries. The presence of upstream shear, under these circumstances, only affects the distribution of the ageostrophic velocities. Yet, the relatively weak upstream deceleration of the airstream, associated with uniform flow, is not significantly altered. Similarly, the vertical depth over which the disturbances decay is also relatively insensitive to the shear δ, and is characterized by the deformation depth D. However, the maximum ageostrophic velocity at the ridge crest and the strength of the forced circulation can be significantly increased when the shear is positive, and these effects are enhanced for higher ridges. Relatively weak circulations are associated with negative shears, and a reversed circulation cell will exist above the ridge when the upstream flow reverses direction aloft. These features are displayed in Fig. 7.

The analysis of flow over finite-amplitude orography is intimately related to important problems in mountain meteorology. These include the interaction of fronts with orographic slopes and the isolation of the physical mechanisms that produce lee cyclogenesis. Further problems that need to be addressed in this regard relate to the stability properties of the solutions, the use of nonisentropic boundaries and the extension to three-dimensional flow.

Acknowledgments. Our appreciation is expressed to Dr. Glen Shutts and Professor Huw Davies for their helpful comments on mountain flows. This study is based on a Masters thesis prepared by Brian Gross at the University of Colorado in Boulder. Financial support is provided by the National Science Foundation under NSF Grants ATM-8313674 and ATM-8418625.

APPENDIX A

The Boundary Conditions

The lower boundary is assumed to be a ridge aligned normally to the basic flow (2), but the ridge may slope in the cross-stream direction $Y = y - \mathrm{Ro}u_g(Z)$. The lower boundary condition, which applies at $Y = 0$, may be expressed in geostrophic coordinates as

$$w = \frac{\epsilon}{D}u_g\frac{\partial h}{\partial X} + \mathrm{Ro}\delta^* v_g, \quad Z = \frac{\epsilon}{D}h(X) \tag{A1}$$

where ϵ represents the height and $h(x)$ the shape of the ridge, D is the deformation depth, and the constant cross-stream slope is represented by the product of a constant $\delta^* < 1$ and the Rossby number. Since u_g is a linear function of height $Z = z$, a constant cross-stream slope of approximately the same magnitude is also directed along the physical space y-axis.

Now (4) and (11) may be combined to give

$$u_g J^{-1} = u_g + u_a^*. \tag{A2}$$

Then, multiplication of (A1) by J^{-1} and introduction of (10) and (A2) yields the lower boundary condition expressed by (13). Similarly, inclusion of a cross-stream slope of the upper boundary surface $\mathrm{Ro}\delta^*$ yields the condition, at $Y = 0$, given by (14).

APPENDIX B

Solutions over Semicircular and Semi-elliptical Ridges in an Unbounded Atmosphere

The solution over a semicircular ridge

$$x^2 + z^2 = \left(\frac{\epsilon}{D}\right)^2, \quad z \geq 0 \tag{B1}$$

has been presented by Gill (1981; Eqs. 5.16–5.18). (The ratio of the horizontal to vertical coordinate is actually $Nf^{-1} \sim 10^2$ in dimensional units.) The solution for v_g is given by

$$\mathrm{Ro}v_g = -\left\{r - \left[r^2 - \left(\frac{\epsilon}{D}\right)^2\right]^{1/2}\right\}(x/r), \tag{B2}$$

where $r^2 = x^2 + z^2$. The ageostrophic velocity component u_a may be determined at the crest ($x = 0$, $z = \epsilon/D$) and at the base ($x = \epsilon/D$, $z = 0$) of the ridge (B1). At both locations $w = 0$, so that $u_a^* = u_a$ in (9). Then u_a is determined by (4), which may be transformed into physical space as

$$u_a = -u_g\frac{\partial \mathrm{Ro}v_g}{\partial X} = -\left(u_g\frac{\partial \mathrm{Ro}v_g}{\partial x}\right)\Big/\left(1 + \mathrm{Ro}\frac{\partial v_g}{\partial x}\right). \tag{B3}$$

Evaluation of $\partial\,\mathrm{Ro}v_g/\partial x$ from (B2) yields $\partial\,\mathrm{Ro}v_g/\partial x = -1$ at $x = 0$: u_a is infinite at the peak of the ridge. Moreover, $\partial\,\mathrm{Ro}v_g/\partial x = \infty$ at $z = 0$, so that $u_a = -u_g$, and the flow is stagnant at the base of the ridge. Similar results have been obtained by Pierrehumbert (1985) using different ridge slopes. However, the *critical* slope that is responsible for $u_a = \infty$ at the crest is inherent in the ridge represented by (B1): the ridge preserves its slope independently of ϵ/D. In addition, there is no justification for the neglect of the advection term $(u_g + u_a)\partial u_a/\partial x$ under these circumstances.

It is possible to eliminate the infinite velocity over the crest by considering a broader ridge. In particular, the semicircular ridge expressed in geostrophic coordinates,

$$X^2 + Z^2 = \left(\frac{\epsilon}{D}\right)^2, \tag{B4}$$

may be obtained from (33b) by setting $\Psi_0 = 0$ and letting $H \to \infty$. Introduction of (B4) into (33a) yields $x = 2X$, so that the ridge in physical space is represented by the semiellipse

$$(x/2)^2 + z^2 = \left(\frac{\epsilon}{D}\right)^2, \quad z \geq 0. \tag{B5}$$

The ageostrophic velocity at the crest of the ridge (B5) may be obtained from (39). This limiting case, $H \to \infty$, provides a finite value, $u_a = u_g$. However, stagnation points still occur at $(x = \pm 2\epsilon/D, z = 0)$ because the slope of the boundary is discontinuous. Elimination of this latter feature is presented in section 4b.

APPENDIX C

Determination of the Lower Boundary

The constant Ψ_0, appearing in (30a), and defined by (44), is the same value at all points along the lower boundary. In particular, the conditions

$$\Psi(0, \epsilon/D + \Psi_0) = \Psi_0, \tag{C1}$$

$$\Psi(1, (\epsilon/D)/2 + \Psi_0) = \Psi_0 \tag{C2}$$

must be satisfied by assigned values of ϵ/D and r. Evaluation of these conditions by means of (43b) determine both the source/sink, strength m and their separation a in terms of ϵ/D and r. Subtraction of (C2) from (C1) yields $\tan^{-1}\theta_1 = 2\tan^{-1}\theta_2$, that is

$$\tan^{-1}\left\{\frac{\sin 2\left[\frac{\pi D}{2H}\left(\frac{\epsilon}{D}+\Psi_0\right)\right]\sinh 2\left(\frac{\pi Da}{2H}\right)}{1-\cos 2\left[\frac{\pi D}{2H}\left(\frac{\epsilon}{D}+\Psi_0\right)\right]\cosh 2\left(\frac{\pi Da}{2H}\right)}\right\} = 2\tan^{-1}\left\{\frac{\sin 2\left[\frac{\pi D}{2H}\left(\frac{\epsilon/D}{2}+\Psi_0\right)\right]\sinh 2\left(\frac{\pi Da}{2H}\right)}{\cosh 2\left(\frac{\pi D}{2H}\right)-\cos 2\left[\frac{\pi D}{2H}\left(\frac{\epsilon/D}{2}+\Psi_0\right)\right]\cosh 2\left(\frac{\pi Da}{2H}\right)}\right\}. \tag{C3}$$

This expression (C3) may be written as

$$\theta_1 = \tan(2\tan^{-1}\theta_2) = 2\theta_2/(1-\theta_2^2). \tag{C4}$$

Equation (C4) may be expressed as a quadratic equation for

$$\beta \equiv \cosh\left(\frac{\pi D}{2H}a\right) \geq 1.$$

The limiting separation $\beta[\epsilon/D, r(0.1)] = 1$, a doublet ridge, is represented by the upper curve in Fig. 3.

Once the separation a is determined from (C4), the source/sink strength m may be found from either (C1) or (C2). Equation (C1) provides the expression

$$m = \frac{\epsilon}{D}\Big/ 2\tan^{-1}\theta_1, \tag{C5}$$

where θ_1 is defined by (C3). A discontinuity in the streamfunction will occur above the mountain crest when θ_1 changes sign. The condition

$$1 - \cos 2\left[\pi D\left(\frac{\epsilon}{D}+\Psi_0\right)\Big/ 2H\right]\cosh 2(\pi Da/2H) = 0 \tag{C6}$$

represents a second limiting expression for values of a, the lower curve in Fig. 3. Further, the argument of the cosine in (C6) ranges between 0 and $\pi/2$ when $0 \leq r \leq 4/9$, for $q = 0.1$. Over this range, a satisfies $0 \leq a \leq \infty$. The other expression for m (C2) also provides a similar constraint. However, the limiting curve falls below the lower curve in Fig. 3.

The values of m and a, so determined, provide the ridges appearing in Figs. 4–7.

REFERENCES

Eliassen, A., and E. Palm, 1961: On the transfer of energy in stationary mountain waves. *Geofys. Publik.*, **22**, 1–23.

Gill, A. E., 1981: Homogeneous intrusions in a rotating stratified field. *J. Fluid Mech.*, **103**, 275–295.

Global Atmospheric Research Program, 1980: *Orographic effects in planetary flows.* GARP Publ. Ser. No. 23, WMO-ICSU, Geneva, 450 pp.

Hoskins, B. J., 1975: The geostrophic momentum approximation and the semigeostrophic equations. *J. Atmos. Sci.*, **32**, 233–242.

——, and F. P. Bretherton, 1972: Atmospheric frontogenesis models: mathematical formulation and solution. *J. Atmos. Sci.*, **29**, 11–37.

——, and I. Draghici, 1977: The forcing of ageostrophic motion according to the semigeostrophic equations and in an isentrophic coordinate model. *J. Atmos. Sci.*, **34**, 1859–1867.

Jacobs, S. J., 1964: On stratified flow over bottom topography. *J. Mar. Res.*, **22**, 223–235.

Merkine, L. O., 1975: Steady finite-amplitude baroclinic flow over long topography in a rotating stratified atmosphere. *J. Atmos. Sci.*, **32**, 1881–1893.

Milne-Thomson, L. M., 1967: *Theoretical Hydrodynamics,* Second ed., Macmillan, 600 pp.

Pierrehumbert, R. T., 1984: Linear results on the barrier effects of mesoscale mountains. *J. Atmos. Sci.*, **41**, 1356–1367.

——, 1985: Stratified semigeostrophic flow over two-dimensional topography in an unbounded atmosphere. *J. Atmos. Sci.*, **42**, 523–526.

——, and B. Wyman, 1985: Upstream effects of mesoscale mountains. *J. Atmos. Sci.*, **42**, 977–1003.

Robinson, A. R., 1960: On two-dimensional flow in a rotating stratified fluid. *J. Fluid Mech.*, **9**, 321–332.

Smith, R. B., 1979: The influence of mountains on the atmosphere. *Advances in Geophysics,* Vol. 21, Academic Press, 87–230.

——, 1979: Some aspects of the quasigeostrophic flow over mountains. *J. Atmos. Sci.*, **36**, 2385–2393.